Available online at www.sciencedirect.com
SCIENCE DIRECT
Journal of Power Sources 148 (2005) 32–42
JOURNAL OF POWER SOURCES
www.elsevier.com/locate/jpowsour

Influence of impurities on the conductivity of composites in the system $(3YSZ)_{1-x}$–$(MgO)_x$

Y. Shiratori [a,*], F. Tietz [a], H.J. Penkalla [b], J.Q. He [c], Y. Shiratori [c], D. Stöver [a]

[a] *Forschungszentrum Jülich, Institute for Materials and Processes in Energy Systems (IWV-1), 52425 Jülich, Germany*
[b] *Forschungszentrum Jülich, Institute for Materials and Processes in Energy Systems (IWV-2), 52425 Jülich, Germany*
[c] *Forschungszentrum Jülich, Institute of Solid State Research (IFF), 52425 Jülich, Germany*

Received 16 April 2004; received in revised form 6 December 2004; accepted 22 January 2005
Available online 28 April 2005

Abstract

$(3YSZ)_{1-x}$–$(MgO)_x$ form composites above $x = 0.15$, which consist of stabilized-zirconia and magnesia. Electrical conductivities of the two-phase composites were measured by the four-probe DC technique. Negative influences of impurities such as SiO_2 on the conductivity are discussed with the aid of microstructural investigations using SEM and TEM. In the investigated composites, the impurities do not directly affect the electrical conduction as current blockers at grain boundaries as usually observed in pure YSZ electrolytes. Microstructural investigation using HRTEM revealed that grain boundaries of the stabilized zirconia are very clean because the silicon and aluminum oxide impurities react with MgO to form discrete Mg_2SiO_4 and $MgAl_2O_4$ grains in the electrolytes, respectively. A theoretical approach taking into consideration continuous volumes of existing phases reveals that the conductivity of the two-phase composites depends on the phase continuity. The reduction of the continuity of the zirconia phase is the main reason for the decrease of conductivity in the present system.

Keywords: Solid oxide fuel cell; Solid electrolytes; Two-phase composite; Electrical conductivity

1. Introduction

Eight mole percent yttria-stabilized zirconia (8YSZ) has a smaller thermal expansion coefficient (TEC) compared to the other component materials for solid oxide fuel cells (SOFCs). The mismatch causes residual stresses resulting in bent or even cracked cells during stack assembling especially in the anode-supported SOFC [1,2]. With a view of more reliable fabrication of SOFCs, composite electrolyte materials composed of zirconia and magnesia were prepared by sintering of powder mixtures at 1400 °C [3].

Grain reported that the MgO concentration in ZrO_2 for full stabilization and maximum solubility is 12.1 and 14.1 mol%, respectively, at 1470 °C [4]. Rohland and Moebius reported the conductivity of magnesia fully stabilized-zirconia (MSZ) [5]. MSZ has maximum conductivity of about 0.06 and 0.02 S cm^{-1} at 900 and 800 °C, respectively. If the admixed MgO amount exceeds the solubility limit, MgO can exist as a second phase in the zirconia matrix after sintering. Because MgO has a larger TEC than that of zirconia, the resulting composite electrolytes show increased TEC values close to the other SOFC materials [3].

In this investigation, commercial 3 mol% yttria-stabilized zirconia (3YSZ) was selected as a starting material for making the composites. 3YSZ was used not only because it is easily available but also because Y^{3+} cations lower the activation energy of ionic conduction of Mg-dissolved zirconias [5,6]. Hellmann and Stubican [7] investigated phase relations in the ternary solid solution of MgO–Y_2O_3–ZrO_2. According to their phase diagram at 1420 °C, the solubility limit of MgO in the yttrium-dissolved zirconia is less than 20 mol%. Recently, Fonseca and Muccillo [8] crystallographically and

* Corresponding author. Present address: Department of Molecular and Material Sciences, Interdisciplinary Graduate School of Engineering Sciences, Kyushu University, 6-1 Kasugakoen, Kasuga, Fukuoka 816-8580, Japan. Tel.: +81 92 583 7527; fax: +81 92 573 0342.
E-mail address: y.shira@mm.kyushu-u.ac.jp (Y. Shiratori).

0378-7753/$ – see front matter © 2005 Elsevier B.V. All rights reserved.
doi:10.1016/j.jpowsour.2005.01.036

electrochemically investigated 8YSZ-magnesia composites. The mixtures of 8YSZ and MgO were sintered at 1350 °C for 0.1 h and the MgO solubility limit of 10 mol% was reported. In contrast to [8], the $(3YSZ)_{1-x}$–$(MgO)_x$ electrolytes were prepared over the wide range of MgO content x and the composite electrolytes composed of fully stabilized zirconia and magnesia were formed.

In this paper, two MgO powders with high and low amounts of silica were used to make the composites. The electrical conductivities of the composites were measured to clarify the influence of impurities on the electrical conduction of the two-phase composite materials. Silica is the most common impurity in ceramic powders and enhances the densification of solid electrolytes through liquid phase sintering [9,10]. Therefore, glassy phases can often be observed at the grain boundaries of zirconia [11]. The glassy phases are well known for their detrimental effect on the electrical property of the electrolytes due to the poor ionic conductivity [12] and result in a significant increase in grain boundary resistance [11–14]. Moreover, it has been reported that Mg-containing silicate phases also crystallized at grain boundaries [14–16]. Leach investigated the behavior of the crystalline phases in the magnesia partially stabilized zirconia system using transmission electron microscopy (TEM) [9] and reported that, at the sintering temperature of 1450 °C, the MgO reacts with silica to form discrete forsterite grains within the zirconia matrix. In the temperature range of 1550–1600 °C, the silicate phase begins to wet the tetragonal zirconia phase.

Also, in the present system the morphology of the grain boundaries needs to be characterized with TEM because of the impurity level of the used MgO powders. The wetting behavior and the chemical interaction with the matrix are the most important information for understanding the influence of the impurities [17,18]. If impurity phases exist at grain boundaries, they will reduce the intergrain contact areas for easier current flow and act as current blockers. In this case, the "brick layer" or "easy path" model can be applied to explain the decrease of conductivity [11,12]. If no impurity phases are detected at the grain boundaries, microstructural investigation can give an explanation for the dependence of electrical conductivity on the amount of impurities by applying the continuity model [19,20].

2. Experimental

The starting powders were 5.3 wt% yttria partially stabilized zirconia (3YSZ) (Unitec Ceramics Ltd.), technical grade MgO (Magnesia 312, Magnesia GmbH) and higher purity MgO (Merck KGaA). The 3YSZ powder contains 0.25 wt% Al_2O_3, 0.12 wt% TiO_2 and 0.03 wt% SiO_2 according to the data sheet of the supplier. The main impurities of the MgO powders obtained by inductively coupled plasma spectroscopy (ICP) are summarized in Table 1. The Magnesia 312 powder (hereafter called MgO-I) contains significant amounts of impurities: 1.55 wt% Ca, 0.19 wt% Fe and 0.18 wt% Si. On the contrary, the MgO powder from Merck (hereafter called MgO-II) is purer than MgO-I and contains 0.26 wt% Na, 0.013 wt% Al and the amount of Si impurity is small (<0.005 wt%). The particle size distributions were measured using a laser particle size analyzer (Fritsch, Germany). The initial average particle size d_{50} was 0.7 μm for 3YSZ, 1.7 μm for MgO-I and 2.0 μm for MgO-II.

Table 1
Main impurities in the two MgO powders obtained by ICP

Element	Amount (wt%)	
	MgO-I	MgO-II
Al	0.017	0.013
Ca	1.55	0.008
Fe	0.19	<0.002
Mn	0.035	<0.001
Na	<0.005	0.26
Si	0.18	<0.005

MgO-I and MgO-II were provided by Magnesia GmbH and Merck KGaA, respectively

Different mixtures of 3YSZ and MgO were wet blended on a rolling bank for 24 h using zirconia balls and ethanol. Then, the suspensions were dried at 60 °C. The nominal content of the MgO mixed with 3YSZ was varied from 0 to 80 mol%. Hereafter, these mixtures are indicated by $(3YSZ)_{1-x}$–$(MgO)_x$ (x: nominal MgO content in the starting mixture). The mixed powders were uniaxially pressed by applying a pressure of 45 MPa. Afterwards, these specimens were sintered at 1400 °C for 5 h in air applying heating and cooling rates of 5 K min^{-1}.

In order to investigate the electrical properties of the $(3YSZ)_{1-x}$–$(MgO)_x$ electrolytes, four-probe DC conductivity measurements were carried out in air in the temperature range from 900 °C down to 200 °C. Four silver wires were fixed on the sintered rectangular specimens (40 mm × 5 mm × 5 mm in size) with silver paste as current and voltage probes. The AC impedance spectroscopy were also applied to gain more information. Sintered cylindrical samples (8 mm in diameter and 2 mm in thickness) were sputtered with platinum on both faces. The measurements were carried out by a Solartron SI-1260 Impedance/Gain phase analyzer in the frequency range of 10 MHz to 50 mHz and in the temperature range of 300–850 °C in air.

The surfaces of the sintered specimens were investigated with a LEO 1530 (Gemini) scanning electron microscope (SEM) equipped with an energy-dispersive X-ray spectrometer (EDS) for microstructural characterization. The mean grain size of zirconia and MgO on the surface was determined by using "analySIS®" software provided by Soft Imaging System GmbH. More than 100 grains on the SEM images covering an area of 26 μm × 18 μm were counted. The polished surfaces were also investigated with SEM and the image analysis software for further microstructural investigations. In the backscattering electron (BSE) images, dark and light gray grains correspond to MgO (insulator) and stabilized zir-

conia grains (conductor), respectively. The images were digitized into pixels with 256 different gray values (0 for black and 255 for white pixels). After setting a gray value as threshold to distinguish the two phases, which is in between the two peaks corresponding to dark and light gray grains in a gray-value histogram, the images were converted into binary white (conductor grains) and black (insulator grains) images.

Raman spectra were recorded on sintered samples (10 mm in diameter and 1 mm in thickness) at room temperature using a Jobin Yvon T64000 spectrometer equipped with a CCD detector. Ar^+ laser excitation with 514.5 nm wavelength and less than 50 mW power at the sample was used to record signals from an irradiation area (~5 μm spot on the sample). In each experiment, 20 scans were collected and averaged. Positions of the Raman bands were determined as Lorentzian profiles by a curve-fitting program equipped with Grams/AI software (Thermo Galactic).

The analytical TEM investigations were carried out with a Philips CM 200T combined with EDS. The focused ion beam (FIB) technique was applied to prepare the analytical TEM samples using a LEO 1540XB with SEM in a single tool. The samples were thinned down to 100 nm with a Ga ion beam.

The zirconia grain boundary structure was investigated by high resolution TEM (HRTEM) using a JEOL 4000EX microscope. The samples were prepared by standard methods, involving mechanical grinding to a thickness of about 0.1 mm, dimpling to about 15 μm, then ion-beam milling to electron transparency on a stage cooled by liquid nitrogen.

3. Results

3.1. Electrical conductivity

The electrical conductivity of the sintered $(3YSZ)_{1-x}$–$(MgO)_x$ with MgO-I measured by the DC four-probe technique is summarized in an Arrhenius diagram (Fig. 1(a)). Fig. 1(b) shows the activation energies of the ionic conduction obtained from the Arrhenius plots as a function of MgO content. At low MgO content, activation energies increase linearly with MgO content. This indicates the dissolution of Mg cations in the YSZ lattice during sintering and reflects the higher association energy between Mg_{Zr}'' and $V_O^{\bullet\bullet}$ and higher migration energy of $V_O^{\bullet\bullet}$ in the zirconia lattice in the presence of the Mg^{2+} ions than expected in the $(Y,Zr)O_2$ binary solid solution [6]. In this sense, convergence of the value of activation energy (approximately 1.37 eV) indicates saturation of MgO in the lattice. The solubility limit of MgO in 3YSZ derived from Fig. 1(b) was approximately 15 mol%. In the X-ray diffractometry of the sintered $(3YSZ)_{1-x}$–$(MgO)_x$, above $x = 0.15$ tiny MgO peaks appeared for both MgO powders and the lattice parameter of the cubic zirconia, which decreases with MgO content in the range of $0.1 \leq x \leq 0.2$, became constant above $x = 0.2$. This fact supports the solubility limit of about 15 mol% and this amount agrees with previously reported values [4,7,8].

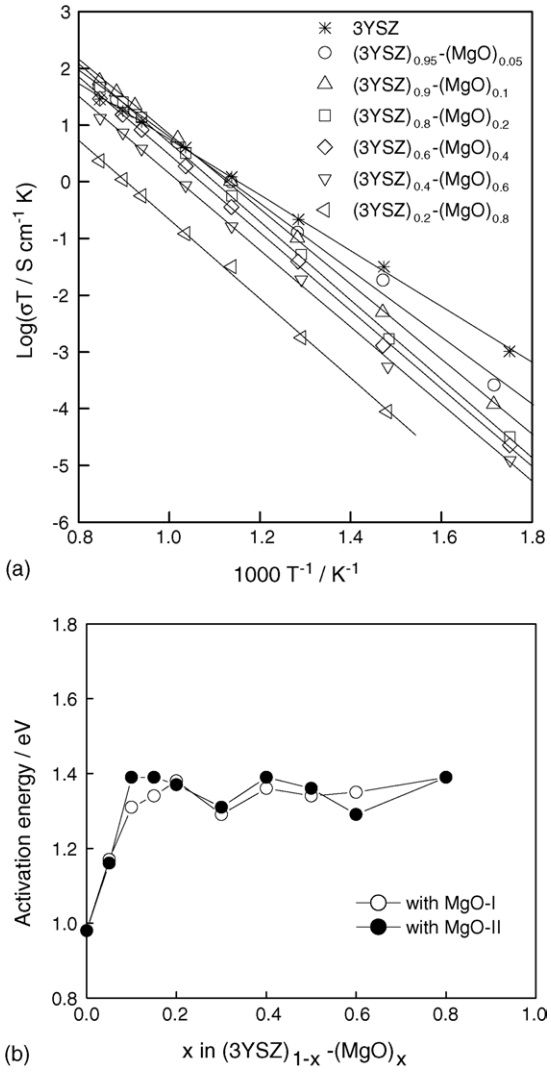

Fig. 1. (a) Arrhenius plot of DC total conductivity for sintered $(3YSZ)_{1-x}$–$(MgO)_x$ samples with MgO-I. (b) Activation energy of the electrical conduction as a function of x. (◯) The samples with MgO-I; (●) the samples with MgO-II.

The conductivities of the $(3YSZ)_{1-x}$–$(MgO)_x$ samples as a function of x at different temperatures are shown in Fig. 2. The $(3YSZ)_{1-x}$–$(MgO)_x$ electrolytes have a maximum conductivity at $x = 0.1$ of 0.054, 0.034 and 0.020 S cm^{-1} at 900, 850 and 800 °C, respectively, comparable to 8YSZ.

As shown in Fig. 2, in the composition range below the solubility limit, there are no significant differences in the conductivity between the samples with MgO-I and MgO-II. At low MgO content, the conductivity increases linearly with x due to an increase in charge carriers in the zirconia lattice resulting from Mg^{2+} dissolution. Above $x = 0.15$, the conductivity decreases with increasing x. The change of the compositional dependence of conductivity can be related to the MgO solubility. Above the solubility limit, the conductivity decreases due to an increase in the insulating MgO phase. At $x \geq 0.2$, the samples with MgO-I systematically showed lower conductivity compared to the samples with MgO-II.

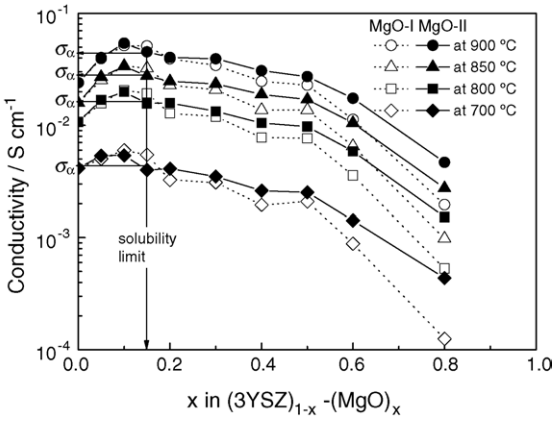

Fig. 2. The DC total conductivity of sintered $(3YSZ)_{1-x}$–$(MgO)_x$ samples as a function of x at different temperatures.

Fig. 3 shows impedance spectra of 3YSZ (a) and $(3YSZ)_{0.8}$–$(MgO)_{0.2}$ with MgO-I (b) measured at 420 °C. The AC impedance measurement of 3YSZ provided three semicircles related to contributions of grain, grain boundary and electrodes in the temperature range of 300–700 °C. However, impedance plots for the composites based on $(3YSZ)_{1-x}$–$(MgO)_x$ showed only one asymmetric large arc and a small electrode contribution. The bulk and grain boundary components could not be clearly resolved. This phenomenon has also been reported for the $(8YSZ)_{1-x}$–$(MgO)_x$ and $(8YSZ)_{1-x}$–$(Al_2O_3)_x$ systems [8,21,22]. In the present system, AC impedance measurements did not give additional information to the DC results.

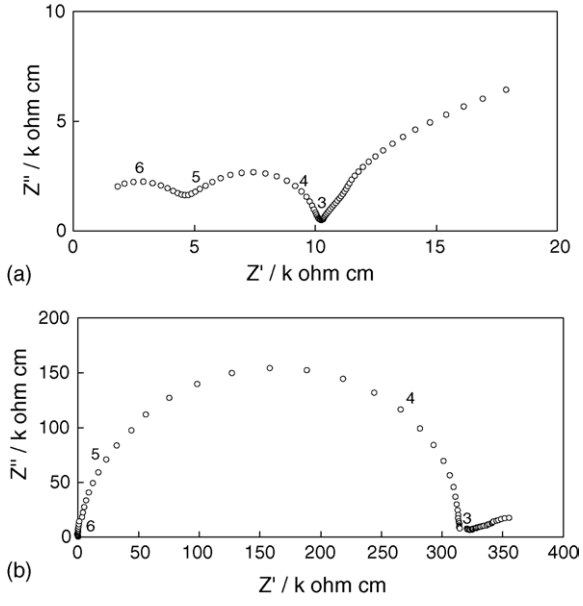

Fig. 3. Impedance spectra of 3YSZ (a) and $(3YSZ)_{0.8}$–$(MgO)_{0.2}$ with MgO-I (b) measured at 420 °C.

3.2. SEM investigation

The microstructures of the electrolytes with different MgO powders were compared with each other. Representative SEM micrographs of the sample surfaces below, near and above the solubility limit are shown in Fig. 4. Below the solubility limit, Fig. 4(a and b), there were no visible differences between the two electrolytes. The electrolytes mainly consist of two types of grains, small $(Y,Zr)O_2$ grains (light gray) and larger $(Y,Mg,Zr)O_2$ grains (dark gray). The bimodal microstructure shows that MgO dissolution in the zirconia promotes grain growth. Near the solubility limit, Fig. 4(c and d), the two electrolytes consist of large cubic $(Y,Mg,Zr)O_2$ grains and small spinel ($MgAl_2O_4$) grains denoted by "YMSZ" and "Sp", respectively, resulting from the reaction between Al_2O_3 impurity in the 3YSZ starting powder and the admixed MgO powders. At this MgO content, a difference in the YMSZ grain structure between the two electrolytes becomes evident. An irregularly shaped surface with tiny grooves is observed on the YMSZ grains when the purer MgO (MgO-II) is selected as a starting material, whereas in the case of the MgO-I the YMSZ grains have a very smooth surface. Above the solubility limit, Fig. 4(e and f), the electrolytes form conductor (YMSZ)–insulator (MgO) binary composites. However, polyhedral grains of magnesium-silicate can be seen as discrete grains only on the surface of the samples with MgO-I. The EDS analysis of these grains gave a Mg:Si ratio of 2:1 indicating the presence of forsterite grains [9].

Mean grain sizes of stabilized zirconia and MgO as a function of x are shown in Fig. 5. The zirconia grain size is strongly influenced by the MgO content, whereas the MgO grain size is nearly constant except for $x = 0.8$. Although MgO dissolution promotes the grain growth of zirconia, an excess of MgO, appearing as second phase in the electrolyte, suppresses the grain growth. In this compositional range ($0.2 \leq x \leq 0.8$), the MgO-I leads to larger zirconia grains than obtained with MgO-II.

3.3. Raman spectroscopy

Raman spectroscopy was applied to detect the structural changes of zirconias because of its higher sensitivity to oxygen displacement than X-ray diffractometry [23]. According to the $k = 0$ factor group analyses for the three different structures of the zirconia, the monoclinic phase (C_{4h}) with four molecules in a unit cell has 18 Raman active modes ($9A_g + 9B_g$), the tetragonal structure (D_{4h}) with two molecules in a unit cell has 6 Raman active modes ($A_{1g} + 2B_{1g} + 3E_g$) and the cubic fully-stabilized phase (O_h) with four molecules in a unit cell has only one Raman active mode of F_{2g} [24,25]. Tetragonal and monoclinic phases have many overlapping bands. However, the two phases can be distinguished by the bands at 148 and 266 cm^{-1} for the tetragonal phase and at 179 and 191 cm^{-1} for the monoclinic phase. The cubic phase has a band at about 605–614 cm^{-1}.

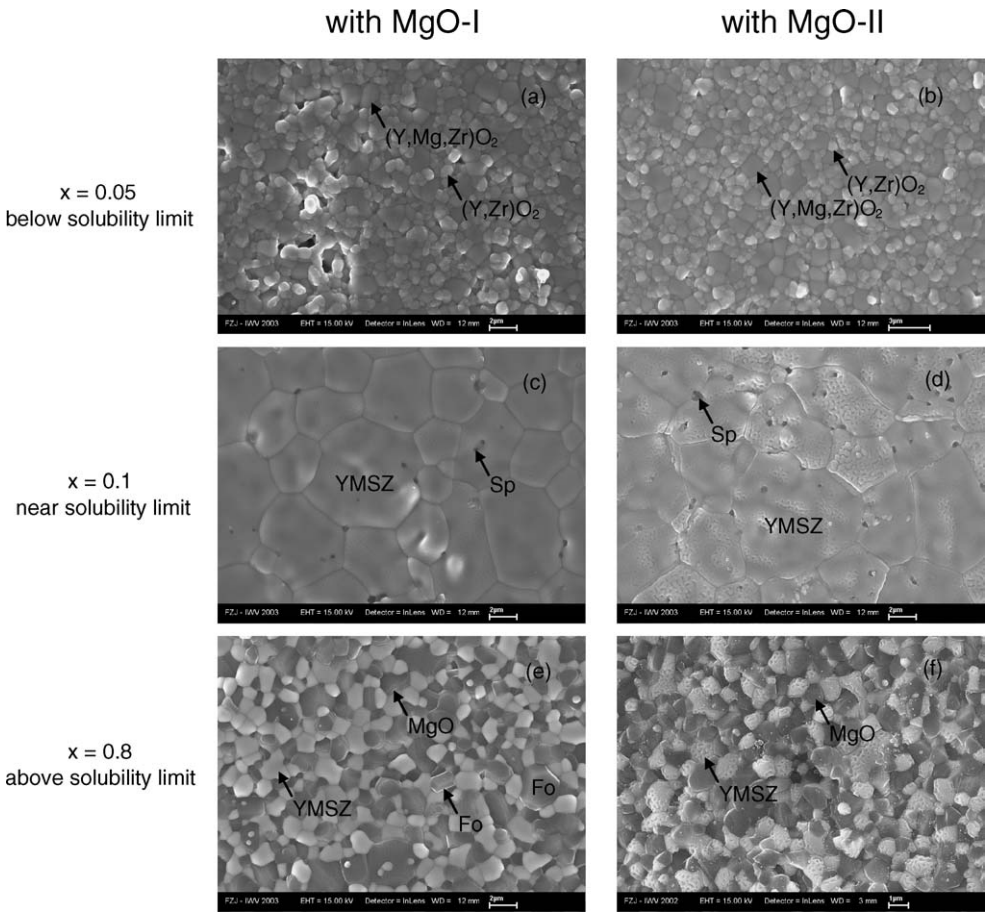

Fig. 4. SEM images of $(3YSZ)_{1-x}$–$(MgO)_x$ sample surfaces with different MgO powders below, near and above the solubility limit of MgO in 3YSZ. All samples were sintered at 1400 °C for 5 h in air. YMSZ: cubic $(Y,Mg,Zr)O_2$; Sp: spinel; Fo: forsterite.

Raman spectra obtained from the sample surfaces of sintered $(3YSZ)_{1-x}$–$(MgO)_x$ specimens with MgO-I are shown in Fig. 6. In the composition range of $0 \leq x \leq 0.07$, only the tetragonal zirconia was detected. When the MgO content exceeds 0.1, the zirconia phase changes from the tetragonal to the cubic structure. The MgO concentration for cubic stabilization obtained by Raman spectroscopy was in good agreement with previously reported values [4,7].

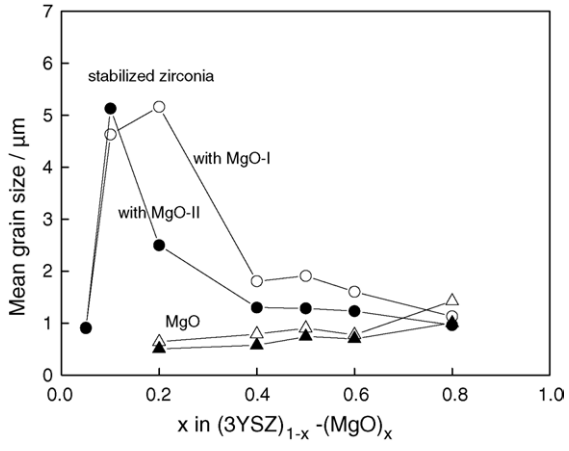

Fig. 5. Mean grain sizes of stabilized zirconia and MgO on the sintered $(3YSZ)_{1-x}$–$(MgO)_x$ sample surfaces as a function of x. (◯), (△) Samples with MgO-I; (●), (▲) samples with MgO-II; 100 grains on the surface were measured for each sample.

In the region of $0.1 \leq x \leq 0.8$, broad bands between 250 and 450 cm^{-1} (Region I) persist, although the factor group analysis indicates only one Raman active mode. These broad bands are due to the breakdown of the $k = 0$ selection rule caused by the dissolution of the Y^{3+} and Mg^{2+} ions into the zirconia lattice, which leads to a disordered cubic lattice [24,25]. The bands at 955, 1008 and 1083 cm^{-1} (Region II) are considered to be fluorescence from rare earth impurities such as Sm, Tb, Ho and Er in the cubic zirconia lattice [24,26]. These three bands become sharp and split at $x \leq 0.07$. The additional sharp bands at 401, 989, 1000, 1062, 1074 and 1088 cm^{-1} (▼) correspond to the fluorescence of rare earth impurities in the tetragonal zirconia lattice [27]. The splitting reflects the site symmetry difference around the impurity cations between the cubic and tetragonal zirconia lattices.

The same phenomena were also observed in the samples with lower silica impurity made of MgO-II. The only difference detected in the Raman spectroscopy with different MgO powders was that MgO-I leads to the formation of the forsterite (Mg_2SiO_4) phase at $x \geq 0.4$. The two bands at

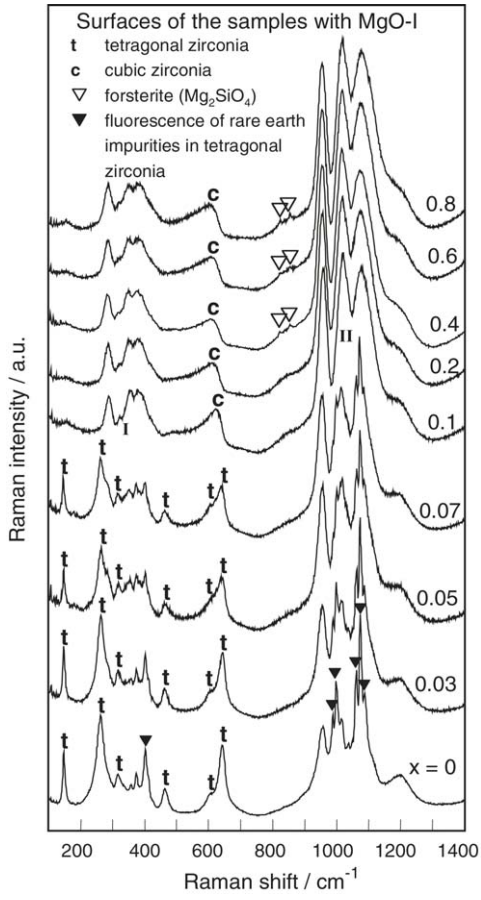

Fig. 6. Raman spectra detected on sintered $(3YSZ)_{1-x}$–$(MgO)_x$ sample surfaces with MgO-I ($0 \le x \le 0.8$).

824 and 856 cm^{-1} (▽) are in good agreement with the bands corresponding to intramolecular Si–O stretching in forsterite [28].

3.4. TEM/HRTEM investigation

According to the literature, the Si and Al impurities form glassy phases melting at about 1300 °C and wetting the zirconia grains [29]. Moreover, in the magnesia partially stabilized zirconia, a crystalline grain boundary silicate (forsterite) is reported at sintering temperatures of above 1600 °C [9]. However, detailed studies by HRTEM did not reveal any intergranular impurity phase in the present system. Fig. 7 shows an HRTEM micrograph at a zirconia grain boundary in the $(3YSZ)_{0.4}$–$(MgO)_{0.6}$ composite with MgO-I. Atom columns are visible on the right side of the picture. The lattice fringes of the right-side grain correspond to the (1 0 1) plane. Impurity phases are absent at the grain boundary region although disorder on the atomic level is observed. Several grain boundaries and multiple grain junctions were investigated. However, no impurity phases were observed.

Fig. 8 shows a typical TEM picture (a) and corresponding element maps based on EDS (b) for the $(3YSZ)_{0.4}$–$(MgO)_{0.6}$

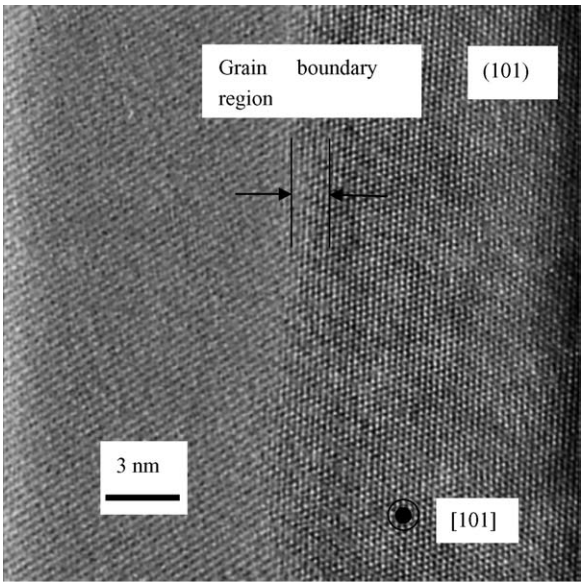

Fig. 7. HRTEM micrograph of a zirconia grain boundary in $(3YSZ)_{0.4}$–$(MgO)_{0.6}$ with MgO-I showing the absence of impurity phases.

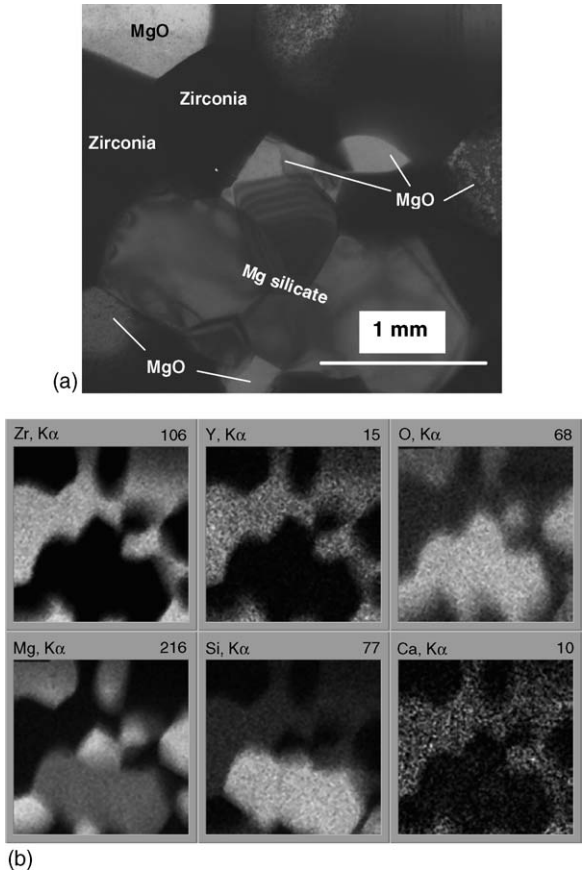

Fig. 8. Typical bright field image (a) and element maps of Zr, Y, O, Mg, Si and Ca obtained by EDS (b) for $(3YSZ)_{0.4}$–$(MgO)_{0.6}$ with MgO-I. In the bright field image, white, light gray and dark gray grains are MgO, Mg-silicate and stabilized zirconia, respectively. In the element maps, the bright pixels indicate higher X-ray (K_α) intensity for each element. The numbers indicate gray values for brightest pixel in the respective maps.

composite with MgO-I. As shown in Fig. 8(a), amorphous glassy phases at the grain boundary multiple junctions and rounded zirconia grain boundaries were not visible, although they were often observed in the presence of SiO_2 impurities [17,18]. The corresponding element maps (Fig. 8(b)) reveal that the MgO phase binds the SiO_2 impurity to form discrete magnesium-silicate grains and CaO enters YMSZ.

In the $(3YSZ)_{1-x}$–$(MgO)_x$ electrolyte, Si-rich impurity phases could not be observed at multiple grain junctions or at zirconia grain boundaries. The silica impurity, which may block some section of the electrical current pathways at the grain boundaries, is sucked into the MgO phase to form magnesium-silicate. The silicate was identified as forsterite by EDS and Raman spectroscopy. The forsterite (Mg_2SiO_4) is a preferential compound compared to enstatite ($MgSiO_3$) because the standard free energies of formation at 298 K for forsterite and enstatite are −63.7 and −36.2 kJ/mol, respectively [10].

4. Discussion

Verkerk et al. reported that in the yttria stabilized-zirconia electrolyte macroscopic grain boundary conductivity increases with increasing zirconia grain size, whereas the grain interior conductivity is constant [30]. Generally, the specific conductivity of the grain boundary (grain-to-grain direct contact without impurity phases) is two orders of magnitude lower than that of the grain interior because of the formation of space charge layers or segregation of dissolved ions [30–32]. Therefore, if the grain boundary thickness and specific grain boundary conductivity are constant, larger grain size leads to higher macroscopic conductivity because of the smaller number of resistive grain boundaries. Furthermore, according to Näfe's theoretical model [33], the macroscopic grain boundary conductivity has no influence on the DC total conductivity due to the small thickness of the grain boundaries. However, in the present system the contrary phenomenon was observed: the enlarged zirconia grains result in lower DC conductivity (see Figs. 2 and 5). In other words, the present system does not strictly follow the general relationship between grain size and conductivity.

From earlier studies in the system ZrO_2–Y_2O_3–MgO, it is known that the cubic ZrO_2–MgO solid solutions, stable only at high temperatures (above 1400 °C), decompose to tetragonal zirconia and magnesia at lower annealing temperatures and subsequently to monoclinic zirconia and magnesia during cooling [5,34]. This decomposition can lead to two or three times larger resistivity [5] and is more detrimental for the ionic conductivity than the impurity influence discussed in this study. The maximum decomposition rate is reached at 1100–1200 °C [5,34] whereas at the operating temperature of anode-supported SOFCs (800 °C or below) the rate might be kinetically negligible because of the quite slow cation diffusion [34,35]. However, during cell production (for example, the cathode materials are sintered on the electrolytes at

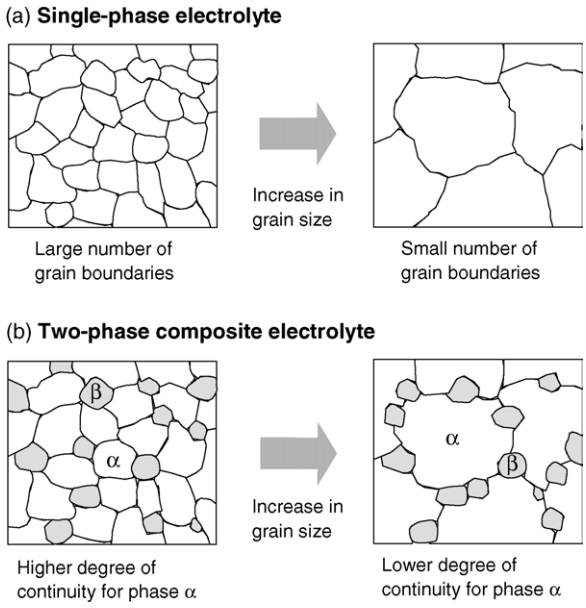

Fig. 9. Influence of grain size on microstructure of single-phase electrolyte (a) and two-phase composite electrolyte (b).

1100–1200 °C) the decomposition may occur. While the aim of this paper is to show the electrical properties of the two-phase composite, this phenomenon has to be monitored carefully in the future work.

Fig. 9 shows a schematic diagram of single-phase electrolyte (a) and two-phase (phases α and β) composite electrolyte (b) with different grain structures. In the case of the single-phase material, as mentioned above, larger grain sizes are equivalent to a smaller number of boundaries and have a positive impact on macroscopic conductivity. In the case of the two-phase composite, as described in Fig. 9(b), an increase in grain size of the phase α (grain size and volume fraction of phase β are assumed to be constant) causes a decrease in continuity of phase α, i.e. phase α with larger grains is more isolated than that with smaller grains. If phase β is an insulator, the reduced continuity of phase α caused by grain coarsening will result in a decrease of conductivity. In the present system, this influence is predominant rather than that described in Fig. 9(a).

Various theoretical approaches represented by the effective media theory (EMT) [36] have been proposed to calculate the electrical conductivity of two-phase composites. EMT only takes into account the volume fractions of the phases and assumes homogeneous microstructures. Fan proposed an approach described by topological parameters [19]. The approach considers not only the effect of volume fraction but also the effect of phase continuity. He transformed a two-phase composite consisting of phases α and β into a body with three microstructural elements. Element I consists only of α grains with a continuous volume fraction of $f_{\alpha c}$ and contains only α–α grain boundaries. Element II consists only of β grains with a continuous volume fraction of $f_{\beta c}$ and contains only β–β grain boundaries. Element III consists of

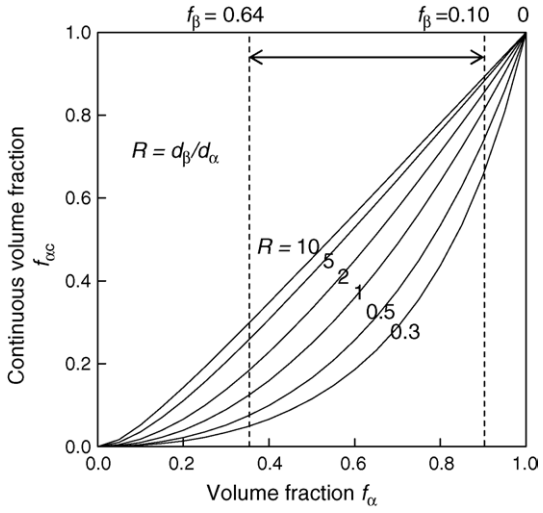

Fig. 10. Correlation between continuous volume fraction $f_{\alpha c}$ and volume fraction f_α as a function of grain size ratio R ($=d_\beta/d_\alpha$).

chains of α and β grains and has only α–β phase boundaries. In this hypothetical model, considering a parallel arrangement of the three resistive elements along an electrical field, the following equation to simulate the conductivity of the two-phase composite can be derived:

$$\sigma_c = \sigma_\alpha f_{\alpha c} + \sigma_\beta f_{\beta c} + \frac{F_s}{f_{\alpha III}/\sigma_\alpha + f_{\beta III}/\sigma_\beta} \quad (1)$$

where σ_c, σ_α and σ_β are conductivities of the composite and of phases α and β, respectively, $f_{\alpha III}$ and $f_{\beta III}$ are volume fractions of the phases α and β in element III, respectively, and F_s is the degree of separation expressed by:

$$F_s = 1 - f_{\alpha c} - f_{\beta c} \quad (2)$$

The continuous volume fractions of respective phases are:

$$f_{\alpha c} = \frac{R f_\alpha^2}{f_\beta + R f_\alpha} \quad (3)$$

$$f_{\beta c} = \frac{f_\beta^2}{f_\beta + R f_\alpha} \quad (4)$$

where f_α and f_β are volume fractions of the phases α and β, respectively, in the two-phase composite ($f_\alpha + f_\beta = 1$) and R is the grain size ratio d_β/d_α (d_α and d_β are the mean grain sizes of the respective phases) [20]. The correlation between continuous volume fraction and volume fraction is shown in Fig. 10 for phase α. $f_{\alpha c}$ is strongly dependent on R. The smaller R (larger grain size of phase α) results in less continuous volume of phase α. Eq. (1) has been validated by comparison with experiments [19] and is reasonable in terms of considering both parallel (first and second terms in Eq. (1)) and series (third term) arrangements of the phases α and β. When the phase β is an insulator ($\sigma_\beta = 0$), the following equation can be derived from Eq. (1),

$$\sigma_c = \sigma_\alpha f_{\alpha c} \quad (5)$$

After all, the conductivity of a conductor–insulator composite can be obtained by correcting the conductivity of the conducting phase with the continuous volume fraction of this phase, namely the effective volume fraction for electrical conduction. Using Eq. (3) and $f_\alpha = 1 - f_\beta$, Eq. (6) is derived:

$$\sigma_c = \frac{\sigma_\alpha R(1 - f_\beta)^2}{f_\beta + R(1 - f_\beta)} \quad (6)$$

The conductivity of the conductor–insulator binary composite can be expressed with the grain size ratio R and the volume fraction of phase β. If R becomes smaller, i.e. the continuous volume of the conducting phase is reduced (see Fig. 10), the conductivity of the composite decreases.

Microstructures of the polished $(3YSZ)_{1-x}$–$(MgO)_x$ samples after binarization of the phases (conductor (YMSZ): white, insulator (MgO): black) with different MgO powders are shown in Fig. 11. To confirm the deviation from the average microstructure, the total area fraction of the black parts A_I was calculated for each sample and was compared to the volume fraction of the MgO second phase f_β calculated by using the MgO solubility limit in 3YSZ of 15 mol% as well as the theoretical densities of stabilized zirconia and MgO obtained by X-ray diffractometry. The values of A_I shown below the respective pictures are close to f_β for all selected pictures. Therefore, the images in Fig. 11 do not deviate significantly from the average microstructure of each sample although agglomerated insulator grains were sometimes observed. Grain boundaries of the same phase cannot be seen in the binary white and black images because gray values of the grain boundaries for conductor–conductor and insulator–insulator are close to those of relevant grains. However, these images show very clearly the state of the phase distributions. Up to $x = 0.6$, the insulator phase is embedded in the conductor matrix for both composites. More inhomogeneous phase distributions are observed for the composites with MgO-I compared to MgO-II. This is due to the larger zirconia grain sizes (see Fig. 5). This indicates that the continuity of the zirconia phase is reduced when the MgO-I is used as starting material (see Fig. 9(b)).

The measured conductivities as a function of f_β are plotted in Fig. 12(a and b) for the composites with MgO-I and MgO-II, respectively. f_β is the MgO volume fraction in the composites when the MgO solubility limit in 3YSZ is regarded as 15 mol%. Eq. (6) was used to calculate the electrical conductivities of the composites. The calculated values were fitted to the experimental values regarding R and σ_α as adjustable parameters. In the fitting procedure, the experimental results at $x = 0.15$ ($f_\beta = 0$) and 0.2 ($f_\beta = 0.03$) were not considered. Only the values in the compositional range of $0.3 \le x \le 0.8$ ($0.10 \le f_\beta \le 0.64$) were taken into account because in this volume fraction range, the grain size ratio R is influential on the continuous volume fraction $f_{\alpha c}$ (see Fig. 10). The calculated results are plotted as solid lines in Fig. 12(a and b). They are in good agreement with the experimental results over the investigated compositional range.

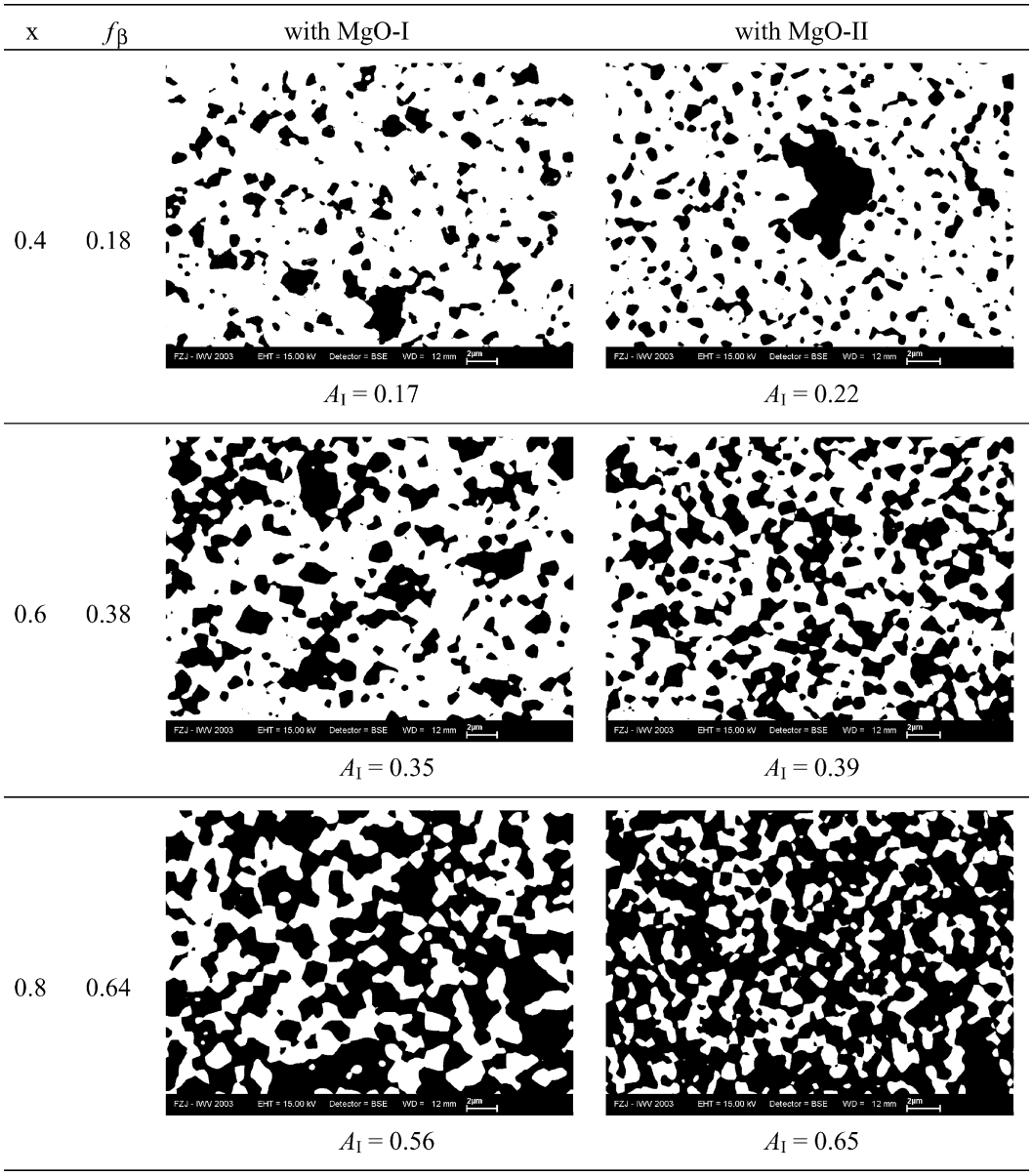

Fig. 11. Conductor (white) and insulator (black) distribution in the composite electrolytes with different MgO powders. A_I is the total area fraction of the black parts in an image and f_β is the volume fraction of the MgO phase calculated by using the MgO solubility limit in 3YSZ of 15 mol% and theoretical densities of the stabilized zirconia and MgO obtained by X-ray diffractometry.

The values of R and σ_α for the composites with MgO-I and MgO-II are listed in Table 2. It is interesting to note that the same values of σ_α were obtained after curve fitting for the composites with MgO-I and MgO-II. These σ_α values for the different temperatures are inserted in Fig. 2 and correspond to the conductivity at which the conductivity starts to decrease with x. The grain size ratio R obtained by the theoretical model, 0.36–0.46 and 0.83–0.96 for the composites with MgO-I and MgO-II, respectively, do not deviate significantly from the measurements for $x \geq 0.4$. The smaller R for the composites with MgO-I confirms the enlarged zirconia grains in the composites with MgO-I and, as a result (according to Fig. 10), a smaller continuous volume of conducting phase (YMSZ) compared to the composite with MgO-II. The microstructural investigations and the application of the continuity theory identified grain coarsening of the zirconia phase induced by the impurities in the starting materials as a reason of the lower conductivity measured in the composites with MgO-I.

Table 2
R and σ_α for the composites with MgO-I and MgO-II

Temperature (°C)	R		σ_α	
	With MgO-I	With MgO-II	With MgO-I	With MgO-II
900	0.46	0.87	0.048	0.049
850	0.41	0.96	0.029	0.029
800	0.36	0.94	0.017	0.017
700	0.38	0.83	0.0044	0.0044

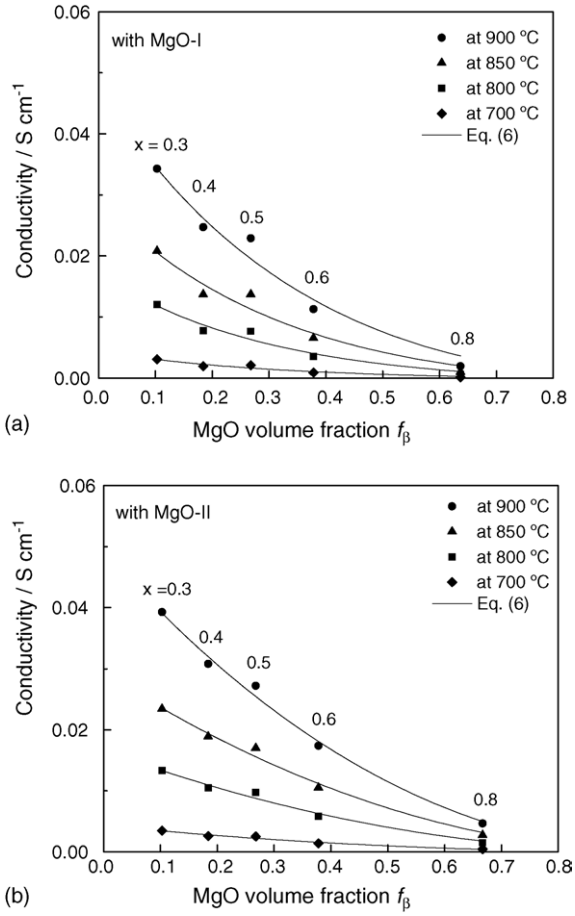

Fig. 12. The DC total conductivity of the sintered $(3YSZ)_{1-x}$–$(MgO)_x$ samples as a function of f_β (volume fraction of MgO phase) at different temperatures. (a) The samples with MgO-I; (b) the samples with MgO-II. The solid lines are theoretical values calculated by Eq. (6) regarding R and σ_α as adjustable parameters (Table 2).

5. Conclusions

The mixtures of 3YSZ and MgO formed composites composed of stabilized zirconia and MgO above 15 mol% MgO after sintering at 1400 °C. The influence of impurities on the conductivity of the composite electrolytes was investigated. In this system, the zirconia grain boundaries were found to be very clean and the impurities (Si and Al) do not act as current blockers because the MgO absorbs the impurities and forms discrete silicate grains at the sintering temperature of 1400 °C. This phenomenon can be used for technical grade raw materials as a chemical strategy to avoid current blocking in technological developments. In the composites based on $(3YSZ)_{1-x}$–$(MgO)_x$, the conductivity is sensitive to the degree of phase continuity. The lower conductivity of the composite electrolytes with MgO-I reflects the decrease in continuity of zirconia phase due to the different impurity level compared with MgO-II. The stability of conductivity with time (and varying Y:Mg ratio) has to be monitored at about 800 °C.

Acknowledgements

The authors gratefully acknowledge the contributions of Mr. Kappertz from IWV-1, Forschungszentrum Jülich, for the preparation of polished samples for microstructural investigations and Ms. Eßer from IWV-2, Forschungszentrum Jülich, for preparation of TEM specimens by FIB. One of the authors (Y. Shiratori, IFF) gratefully acknowledges the Alexander von Humboldt Foundation (Bonn, Germany) for granting financial support through a Research Fellowship.

References

[1] F. Tietz, Thermal expansion of SOFC materials, Ionics 5 (1999) 129–139.
[2] H. Yakabe, Y. Baba, T. Sakurai, Y. Yoshitaka, Evaluation of the residual stress for anode-supported SOFCs, J. Power Sources 135 (2004) 9–16.
[3] Y. Shiratori, F. Tietz, H.P. Buchkremer, D. Stöver, YSZ–MgO composite electrolyte with adjusted thermal expansion coefficient to other SOFC components, Solid State Ionics 164 (2003) 27–33.
[4] C.F. Grain, Phase relations in the ZrO_2–MgO system, J. Am. Ceram. Soc. 50 (1967) 288–290.
[5] R. Rohland, H.H. Moebius, Leitfaehigkeits- und Stabilitaetsuntersuchungen an Festelektrolyten fuer Brennstoffzellen aus dem System ZrO_2–$YO_{1.5}$–MgO, Abh. Saechs. Akad. Wiss., Leipzig, Math.-Naturwiss. Kl. 49 (1968) 355–366.
[6] W.C. Mackrodt, P.M. Woodrow, Theoretical estimates of point defect energies in cubic zirconia, J. Am. Ceram. Soc. 69 (1986) 277–280.
[7] J.R. Hellmann, V.S. Stubican, Phase relations and ordering in the systems MgO–Y_2O_3–ZrO_2 and CaO–MgO–ZrO_2, J. Am. Ceram. Soc. 66 (1983) 265–267.
[8] F.C. Fonseca, R. Muccillo, Impedance spectroscopy of (yttria-stabilized zirconia)–magnesia ceramic composites, Solid State Ionics 131 (2000) 301–309.
[9] C.A. Leach, Sintering of magnesium partially stabilized zirconia—behaviour of an impurity silicate phase, Mater. Sci. Technol. 3 (1987) 321–324.
[10] J. Drennan, R.H.J. Hannink, Effect of SrO additions on the grain-boundary microstructure and mechanical properties of magnesia-partially-stabilized zirconia, J. Am. Ceram. Soc. 69 (1986) 541–546.
[11] M. Gödickemeier, B. Michel, A. Orliukas, P. Bohac, K. Sasaki, L. Gauckler, H. Heinrich, P. Schwander, G. Kostorz, H. Hofmann, O. Frei, Effect of intergranular glass films on the electrical conductivity of 3Y-TZP, J. Mater. Res. 9 (1994) 1228–1240.
[12] S.P.S. Badwal, Grain boundary resistivity in zirconia-based materials: effect of sintering temperatures and impurities, Solid State Ionics 76 (1995) 67–80.
[13] C.C. Appel, N. Bonanos, Structural and electrical characterization of Silica-containing yttria-stabilized zirconia, J. Eur. Ceram. Soc. 19 (1999) 847–851.
[14] S.P.S. Badwal, S. Rajendran, Effect of micro- and nano-structures on the properties of ionic conductors, Solid State Ionics 70/71 (1994) 83–95.
[15] M. Rühle, A. Strecker, D. Waidelich, B. Kraus, In situ observations of stress-induced phase transformations in ZrO_2-containing ceramics, in: N. Claussen, M. Rühle, A.H. Heuer (Eds.), Proceedings of the Second International Conference on the Science and Technology of Zirconia, Stuttgart, American Ceramic Society, Columbus, OH, June 21–23, 1983, pp. 256–274.
[16] K.H. Westmacott, A. Thorel, D. Broussaud, J.Y. Laval, Microstructural changes in (Mg)PSZ during aging at 1000 °C, Ultramicroscopy 22 (1987) 15–26.

[17] Y. Ikuhara, T. Yamamoto, A. Kuwabara, H. Yoshida, T. Sakuma, Structure and chemistry of grain boundaries in SiO_2-doped TZP, Sci. Tech. Adv. Mater. 2 (2001) 411–424.
[18] L. Gremillard, T. Epicier, J. Chevalier, G. Fantozzi, Microstructural study of silica-doped zirconia ceramics, Acta Mater. 48 (2000) 4647–4652.
[19] Z. Fan, A new approach to the electrical resistivity of two-phase composites, Acta Metall. Mater. 43 (1995) 43–49.
[20] Z. Fan, A.P. Miodownik, P. Tsakiropoulos, Microstructural characterization of two phase materials, Mater. Sci. Technol. 9 (1993) 1094–1100.
[21] A.J. Feighery, J.T.S. Irvine, Effect of alumina additions upon electrical properties of 8 mol.% yttria-stabilized zirconia, Solid State Ionics 121 (1999) 209–216.
[22] I.N. Sora, C. Schmid, G. Dotelli, R. Ruffo, C.M. Mari, Analysis of the electrical behaviour of conductor/insulator composites using effective medium theories, J. Eur. Ceram. Soc. 22 (2002) 1645–1652.
[23] M. Yashima, S. Sasaki, M. Kakihana, Y. Yamaguchi, H. Arashi, M. Yoshimura, Oxygen-induced structural change of the tetragonal phase around the tetragonal-cubic phase boundary in ZrO_2–$YO_{1.5}$ solid solutions, Acta Cryst. B50 (1994) 663–672.
[24] N.K. Jensen, R.W. Berg, F.W. Poulsen, Raman spectroscopic characterization of ZrO_2 and Yttrium stabilized zirconias, in: B. Thorstensen (Ed.), Proceedings of the Second European SOFC Forum, Oslo, Norway, European SOFC Forum, Oberrohrdorf, Switzerland, May 6–10, 1996, pp. 647–656.
[25] C.H. Perry, D.W. Liu, R.P. Ingel, Phase characterization of partially stabilized zirconia by Raman spectroscopy, J. Am. Ceram. Soc. 68 (1985) C-184–C-187.
[26] G.H. Dieke, Spectra and Energy Levels of Rare Earth Ions in Crystals, Interscience Publishers, New York, 1968.
[27] N. Maeda, N. Wada, H. Onoda, A. Maegawa, K. Kojima, Spectroscopic properties of Er^{3+} in sol–gel derived ZrO_2 films, Thin Solid Films 445 (2003) 382–386.
[28] B.A. Kolesov, J.V. Tanskaya, Raman spectra and cation distribution in the lattice of olivines, Mater. Res. Bull. 31 (1996) 1035–1044.
[29] G. Wahlberg, L.K.L. Falk, G.L. Dunlop, K.-O. Axelsson, The intergranular microstructure of a partially stabilized ZrO_2 material, J. Mater. Sci. Lett. 4 (1985) 1353–1355.
[30] M.J. Verkerk, B.J. Middelhuis, A.J. Burggraaf, Effect of grain boundaries on the conductivity of high-purity ZrO_2–Y_2O_3 ceramics, Solid State Ionics 6 (1982) 159–170.
[31] X. Guo, Z. Zhang, Grain size dependent grain boundary defect structure: case of doped zirconia, Acta Mater. 51 (2003) 2539–2547.
[32] C. Tian, S.W. Chan, Ionic conductivities, sintering temperatures and microstructures of bulk ceramic CeO_2 doped with Y_2O_3, Solid State Ionics 134 (2000) 89–102.
[33] H. Näfe, Ionic conductivity of ThO_2- and ZrO_2-based electrolytes between 300 and 2000 K, Solid State Ionics 13 (1984) 255–263.
[34] T.H. Etsell, S.N. Flengas, Chem. Rev. 70 (1970) 339–376.
[35] M. Yashima, M. Kakihana, M. Yoshimura, Metastable-stable phase diagrams in the zirconia-containing systems utilized in solid-oxide fuel cell application, Solid State Ionics 86–88 (1996) 1131–1149.
[36] D.S. McLachlan, M. Blaszkiewicz, R.E. Newnham, Electrical resistivity of composites, J. Am. Ceram. Soc. 73 (1990) 2187–2203.